Double-Higher-Order Large-Domain Volume/Surface Integral Equation Method for Analysis of Composite Wire-Plate-Dielectric Antennas and Scatterers

Elene Chobanyan, *Student Member, IEEE*, Milan M. Ilić, *Member, IEEE*, and Branislav M. Notaroš, *Senior Member, IEEE*

***Abstract*—A novel double-higher-order large-domain Galerkin-type method of moments based on higher order geometrical modeling and higher order current modeling is proposed for analysis of composite dielectric and metallic radiation/scattering structures combining the volume integral equation (VIE) approach for dielectric parts and the surface integral equation (SIE) approach for metallic parts of the structure. The technique employs Lagrange-type interpolation generalized hexahedra and quadrilaterals of arbitrary geometrical-mapping orders for the approximation of geometry and hierarchical divergence-conforming polynomial vector basis functions of arbitrary expansion orders for the approximation of currents within the elements. The double-higher-order VSIE (VIE-SIE) method is extensively validated and evaluated against the analytical solutions and the numerical results obtained by alternative higher order methods.**

***Index Terms*—Antennas, curved parametric elements, electromagnetic analysis, higher order modeling, method of moments, numerical techniques, polynomial basis functions, scattering, volume integral equations, wire-plate-dielectric structures.**

I. Introduction

THE method of moments (MoM) for discretizing integral equations in electromagnetics is an extremely powerful and versatile general numerical methodology for electromagnetic-field simulation in antenna and scattering applications [1]–[5]. For antennas and scatterers composed of metallic and homogeneous linear dielectric parts, the MoM is most frequently applied in conjunction with the surface integral equation (SIE) approach [2], [6], [7], where both electric and magnetic equivalent (artificial) surface currents appear as unknowns in SIEs. An alternative approach to MoM analysis of dielectric scatterers is the volume integral equation (VIE) approach [8]–[11], where, employing the volume equivalence principle, a structure containing linear dielectric materials of arbitrary inhomogeneity and complexity is represented by a distribution of unknown volume electric (polarization and conduction) current (the real current) radiating in free space. The analysis of composite dielectric and metallic radiation/scattering structures can be performed combining the VIE for dielectric parts and the SIE for metallic parts, giving rise to a hybrid VIE-SIE or VSIE formulation, which solves simultaneously for the volume current throughout the dielectric domains and the surface current over the metallic surfaces of the composite structure [12]–[14].

However, practically all the existing three-dimensional (3-D) MoM-VIE and MoM-VSIE simulation tools for dielectric/metallic structures are low-order or small-domain (subdomain) techniques—the structure is modeled by volume (and surface) geometrical elements that are electrically very small and the volume (and surface) electric currents within the elements are approximated by low-order (zeroth-order and first-order) basis functions. More precisely, the elements (cells and patches) are on the order of $\lambda/10$ in each dimension, λ being the wavelength in the medium. This results in a very large number of unknowns (unknown current-distribution coefficients) needed to obtain results of satisfactory accuracy, with all the associated problems and enormous requirements in computational resources. In addition, commonly used 3-D VIE elements are in the form of cubes, bricks (parallelepipeds), and tetrahedra, all with planar sides, and thus they do not provide enough flexibility and efficiency in modeling of structures with pronounced curvature.

An alternative which can greatly reduce the number of unknowns for a given problem and enhance further the accuracy and efficiency of the MoM-VIE analysis in antenna/scattering applications is the higher order or large-domain (entire-domain) computational approach [15]. According to this approach, a structure is approximated by a number of as large as possible geometrical elements, and the approximation of current (or field) components within individual elements is in the form of a single (three-fold) functional series of sufficiently high order. Only relatively recently the computational electromagnetics (CEM) community has started to extensively investigate and employ higher order surface and volume elements and higher order basis functions in the frame of MoM, including the SIE formulation [16]–[19], VIE approach [20]–[29], and VSIE hybrid [30]–[34], as well as the finite element method (FEM) [35]–[38].

This paper proposes a novel higher order and large-domain Galerkin-type MoM-VIE technique for 3-D analysis of

Manuscript received April 02, 2012; revised June 15, 2013; accepted August 23, 2013. Date of publication September 10, 2013; date of current version November 25, 2013. This work was supported by the National Science Foundation under Grant ECCS-1002385 and by the Serbian Ministry of Education and Science under grant TR-32005.

E. Chobanyan and B. M. Notaroš are with Colorado State University, Department of Electrical and Computer Engineering, Fort Collins, CO 80523-1373 USA (e-mail: elene.chobanyan@colostate.edu; notaros@colostate.edu).

M. M. Ilić is with University of Belgrade, School of Electrical Engineering, 11120 Belgrade, Serbia and with the Colorado State University, Department of Electrical and Computer Engineering, Fort Collins, CO 80523-1373 USA (e-mail: milanilic@etf.rs).

Color versions of one or more of the figures in this paper are available online at http://ieeexplore.ieee.org.

Digital Object Identifier 10.1109/TAP.2013.2281360

radiation/scattering structures based on higher order geometrical modeling and higher order current modeling, which we refer to as a double-higher-order VIE method. The volume geometrical elements are Lagrange-type interpolation generalized hexahedra of arbitrary geometrical-mapping orders. The basis functions for volume currents are hierarchical divergence-conforming 3-D polynomial vector basis functions of arbitrary expansion orders. The method enables as large as about $2\lambda \times 2\lambda \times 2\lambda$ VIE generalized hexahedra with curvature modeling using high (e.g., fourth) geometrical-mapping orders and p-refined current distributions of high (e.g., sixth) orders of basis functions. Additionally, a whole spectrum of element sizes, geometrical orders, and current-approximation orders can be used at the same time in a single simulation model of a complex structure, making this method essentially a combined, low-to-high, order method and enabling hp-refinement of solutions.

The proposed technique represents a generalization of the MoM-VIE technique [21], where trilinear hexahedra (volume elements of the first geometrical order) are used with higher order polynomial current expansions. It also represents a VIE version of the double-higher-order SIE method [17], on one side, and a MoM version of the double-higher-order FEM [37], on the other side. In fact, this is a double-higher-order VIE-SIE or VSIE method, as it includes the corresponding SIE discretization of metallic surfaces, and in that sense may be considered a generalization of the MoM-VSIE technique [30], which uses volume and surface elements of the first geometrical order in conjunction with polynomial large-domain volume and surface current approximations.

On the other hand, when compared with the alternative higher order VIE and VSIE scattering techniques [24]–[29], [33], and [34], the proposed technique is a wire-plate-dielectric antenna/scattering code. In addition, the present work demonstrates a dramatic improvement of results when using geometrical modeling of the 4th order instead of the 2nd order geometrical modeling, as well as the first single-element, literally entire-domain, models of 3-D scatterers of general shapes (note that such an entire-domain solution to open-region problems is unique not only looking at existing VIE methods but at all available CEM methods overall). Other examples demonstrate versatility of the proposed method in analysis of electrically larger and more complex and practical structures.

Section II of this paper presents the theoretical background and numerical components of the new double-higher-order VSIE technique. In Section III, the technique is validated and its accuracy and efficiency evaluated and discussed in several characteristic examples.

II. Novel Double-Higher-Order VSIE Method for Composite Dielectric/Metallic Structures

A. Two-Potential Volume Integral Equation Formulation for the Equivalent Displacement Vector

Consider an electromagnetic structure consisting of arbitrarily shaped dielectric and metallic parts, situated in free space. Let the relative permittivity, ε_{r}, and conductivity, σ, of the dielectric material be known functions of position, while the permeability at all points is μ_0. In addition, let the structure be excited by a time-harmonic electromagnetic field of complex electric field intensity vector $\mathbf{E}_{\mathrm{i}}$ and angular frequency ω. This field may be a combination of incident plane waves (for a scattering structure) or the impressed field of one or more lumped generators (for an antenna structure). It induces volume electric (polarization and conduction) current, of density $\mathbf{J}$, to flow throughout the volume of the structure. This current and the associated charge are, in turn, the sources of the scattered electric field, of intensity vector $\mathbf{E}_{\mathrm{s}}$. From the constitutive equation for the current, $\mathbf{J}$ is related to the total electric field intensity at any point in the material as [21]

$$\begin{aligned} \mathbf{J} &= \mathrm{j}\omega C\mathbf{D} = \mathrm{j}\omega(\varepsilon_{\mathrm{e}} - \varepsilon_0)(\mathbf{E}_{\mathrm{i}} + \mathbf{E}_{\mathrm{s}}) \\ C &= \frac{\varepsilon_{\mathrm{e}} - \varepsilon_0}{\varepsilon_{\mathrm{e}}}, \quad \varepsilon_{\mathrm{e}} = \varepsilon - \mathrm{j}\frac{\sigma}{\omega} \end{aligned} \tag{1}$$

where $\mathbf{D} = \varepsilon_{\mathrm{e}}\mathbf{E}$ is the equivalent electric displacement vector, and ε_{e} and C are the equivalent complex permittivity and electric contrast (with respect to free space), respectively, of the material at that point. The scattered field can be computed as if the sources were radiating in free space (volume equivalence principle), using Lorenz potentials

$$\mathbf{A} = \mu_0 \int_V \mathbf{J} g \mathrm{d}V \tag{2}$$

$$\Phi = \frac{\mathrm{j}}{\omega\varepsilon_0}\left[\int_V \nabla' \cdot \mathbf{J} g \mathrm{d}V + \int_{S_{\mathrm{d}}} \mathbf{n} \cdot (\mathbf{J}_1 - \mathbf{J}_2) g \mathrm{d}S\right]. \tag{3}$$

Here, V is the domain with volume current and charge (∇' operates on sources $\mathbf{J}$ as a function of primed coordinates only), S_{d} are surfaces of discontinuity in ε_{e} (where surface charge may accumulate), with the unit normal vector, $\mathbf{n}$, directed from medium 2 (with current $\mathbf{J}_2$) into medium 1 (with current $\mathbf{J}_1$), and g is the free-space Green's function

$$g = \frac{e^{-\mathrm{j}\beta_0 R}}{4\pi R}, \quad \beta_0 = \omega\sqrt{\varepsilon_0\mu_0} \tag{4}$$

β_0 being the free-space wave number and R the distance of the field point from the source point. With this, (1) gives the following two-potential VIE with $\mathbf{D}$ as unknown:

$$\frac{\mathbf{D}}{\varepsilon_{\mathrm{e}}} + \mathrm{j}\omega\mathbf{A} + \nabla\Phi = \mathbf{E}_{\mathrm{i}}. \tag{5}$$

Note that if divergence-conforming bases are used in the VIE model, it is advantageous to discretize $\mathbf{D}$, or, in fact, the equivalent displacement current density, $\mathbf{J}_{\mathrm{d}} = \mathrm{j}\omega\mathbf{D}$, in place of $\mathbf{J}$, because the normal component of $\mathbf{D}$ is continuous ($\mathbf{n} \cdot \mathbf{D_1} = \mathbf{n} \cdot \mathbf{D_2}$) across the surfaces S_{d}.

On metallic surfaces—that may have distributed loadings, the volume current density $\mathbf{J}$ degenerates into the surface current density, $\mathbf{J}_{\mathrm{S}}$, and the VIE (5) into a SIE given by [30]

$$Z_{\mathrm{S}}\mathbf{J}_{\mathrm{S}} + \mathrm{j}\omega\mathbf{A}_{\mathrm{tang}} + (\nabla\Phi)_{\mathrm{tang}} = (\mathbf{E}_{\mathrm{i}})_{\mathrm{tang}} \tag{6}$$

where Z_{S} is the appropriate surface impedance. For bare surfaces made of a perfect electric conductor (PEC), $Z_{\mathrm{S}} = 0$, and the tangential component of the total electric field on the surface is zero. In analysis of structures composed of both dielectric and

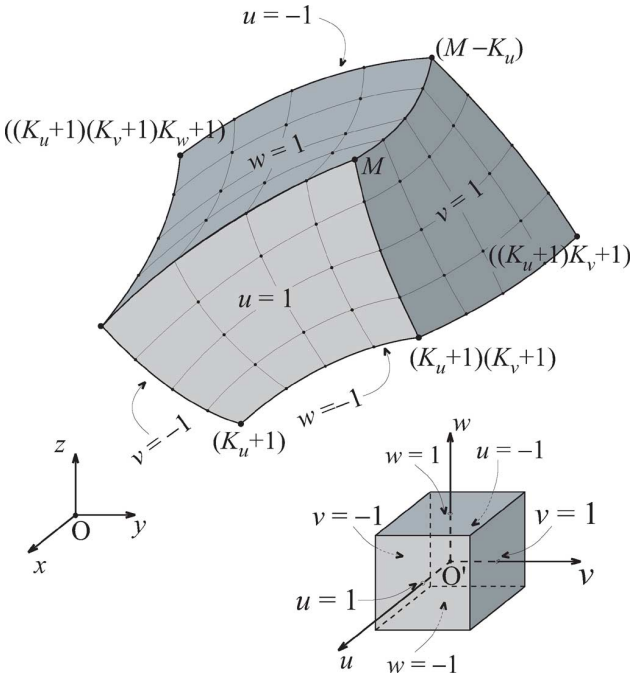

Fig. 1. Generalized curved parametric hexahedral VIE element of geometrical orders K_u, K_v, and K_w ($K_u, K_v, K_w \geq 1$), determined by $M = (K_u + 1)(K_v+1)(K_w+1)$ interpolation nodes arbitrarily positioned in space; cubical parent domain is also shown.

metallic parts, (5) and (6) constitute a hybrid VIE-SIE or VSIE system of integral equations, which are coupled together because potentials $\mathbf{A}$ and Φ at any point of the structure are functions of both $\mathbf{D}$ and $\mathbf{J}_{\mathrm{S}}$. We discretize and solve the VSIE system simultaneously for $\mathbf{D}$ and $\mathbf{J}_{\mathrm{S}}$ using the method of moments.

B. Higher Order 3-D Geometrical Modeling and Higher Order Basis Functions for Volume Current Modeling

As basic building blocks for geometrical modeling in 3-D VIE computations, we propose Lagrange-type generalized curved parametric hexahedral volume elements of arbitrary geometrical orders K_u, K_v, and K_w ($K_u, K_v, K_w \geq 1$), determined by $M = (K_u + 1)(K_v + 1)(K_w + 1)$ points (interpolation nodes) arbitrarily positioned in space and analytically described as [37]

$$\begin{aligned}\mathbf{r}(u,v,w) &= \sum_{i=0}^{K_u}\sum_{j=0}^{K_v}\sum_{k=0}^{K_w} \tilde{\mathbf{r}}_{ijk} L_i^{K_u}(u) L_j^{K_v}(v) L_k^{K_w}(w) \\ &= \sum_{i=0}^{K_u}\sum_{j=0}^{K_v}\sum_{k=0}^{K_w} \mathbf{r}_{ijk} u^i v^j w^k \\ L_i^{K_u}(u) &= \prod_{\substack{l=0 \\ l\neq i}}^{K_u} \frac{u-u_l}{u_i-u_l}, \quad -1 \leq u,v,w \leq 1 \end{aligned} \tag{7}$$

where $\tilde{\mathbf{r}}_{ijk} = \mathbf{r}(u_i, v_j, w_k)$ are position vectors of interpolation nodes, $L_i^{K_u}$ represent Lagrange interpolation polynomials in the u coordinate, with the nodes defined as $u_l = (2l - K_u)/K_u$, $l = 0, 1, \ldots, K_u$, and similarly for $L_j^{K_v}(v)$ and $L_k^{K_w}(w)$, and $\mathbf{r}_{ijk}$ are constant vector coefficients related to $\tilde{\mathbf{r}}_{ijk}$. Note that the orders K_u, K_v, and K_w can be adopted anisotropically (i.e., they do not need to be the same) within an element. Equation (7) defines a mapping from a cubical parent domain to the generalized hexahedron, as illustrated in Fig. 1.

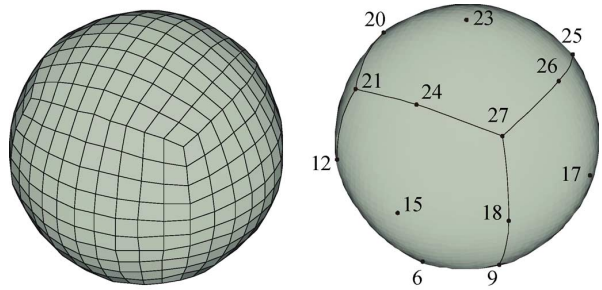

Fig. 2. A sphere modeled by (a) 1000 trilinear hexahedra [$K_u = K_v = K_w = 1$ in (7)] and (b) a single triquadratic hexahedron [$K_u = K_v = K_w = 2$ in (7)].

Geometrically higher order elements obviously allow better flexibility and accuracy in modeling of complex curved structures. As a simple example, Figs. 2(a) and (b) show a sphere modeled by 1000 trilinear hexahedra ($K_u = K_v = K_w = 1$) and a single triquadratic hexahedron ($K_u = K_v = K_w = 2$), respectively. In this paper, we use the equidistant distribution of interpolation nodes along each coordinate in the 3-D parametric space, while the use of specific non-equidistant node distributions, which would provide additional modeling flexibility and accuracy in some VIE applications, is possible as well. In addition, any other choice of higher order volume expansions for geometrical modeling that can be represented as a triple sum of 3-D power functions $u^i v^j w^k$ (e.g., parametric hexahedra using spline functions for describing the geometry) can also readily be implemented in our VIE method.

We represent the displacement vector inside every generalized hexahedron (Fig. 1) in the model as [21]

$$\begin{aligned}\mathbf{D} = &\sum_{p=0}^{N_u}\sum_{s=0}^{N_v-1}\sum_{t=0}^{N_w-1} \alpha_{upst}\mathbf{f}_{upst} + \sum_{p=0}^{N_u-1}\sum_{s=0}^{N_v}\sum_{t=0}^{N_w-1} \alpha_{vpst}\mathbf{f}_{vpst} \\ &+ \sum_{p=0}^{N_u-1}\sum_{s=0}^{N_v-1}\sum_{t=0}^{N_w} \alpha_{wpst}\mathbf{f}_{wpst}\end{aligned} \tag{8}$$

where $\mathbf{f}$ are divergence-conforming hierarchical-type vector basis functions defined by

$$\begin{aligned}\mathbf{f}_{upst} &= \frac{Q_p(u)v^s w^t}{\Im}\mathbf{a}_u \\ \mathbf{f}_{vpst} &= \frac{u^p Q_s(v) w^t}{\Im}\mathbf{a}_v \\ \mathbf{f}_{wpst} &= \frac{u^p v^s Q_t(w)}{\Im}\mathbf{a}_w \\ Q_p(u) &= \begin{cases} 1-u & p=0 \\ u+1 & p=1 \\ u^p-1 & p\geq 2, \text{even} \\ u^p-u & p\geq 3, \text{odd} \end{cases} \\ &\qquad -1 \leq u,v,w \leq 1\end{aligned} \tag{9}$$

N_u, N_v, and N_w are the adopted orders of the polynomial current approximation in the u-, v-, and w-direction, respectively, which are entirely independent from the element geometrical

orders (K_u, K_v, and K_w), $\{\alpha\}$ are unknown current-distribution coefficients, and $\Im$ is the Jacobian of the covariant transformation, found from unitary vectors $\mathbf{a}_u$, $\mathbf{a}_v$ and $\mathbf{a}_w$ along the parametric coordinates

$$\Im = (\mathbf{a}_u \times \mathbf{a}_v) \cdot \mathbf{a}_w, \quad \mathbf{a}_u = \frac{\partial \mathbf{r}}{\partial u}, \quad \mathbf{a}_v = \frac{\partial \mathbf{r}}{\partial v}$$
$$\mathbf{a}_w = \frac{\partial \mathbf{r}}{\partial w} \tag{10}$$

with $\mathbf{r}$ given in (7). Basis functions defined in (9) are hierarchical functions (each lower-order set of functions is a subset of all higher-order sets). Note that, although orders N_u, N_v, and N_w can be arbitrary, values up to 6 (or slightly higher) are generally used to ensure optimal convergence [39].

Note that the lowest order of approximation ($N_u = N_v = N_w = 1$) in (8)–(10) yields the 3-D rooftop functions on generalized hexahedral cells (which, for such basis functions, then must be very small). For any s and t ($0 \le s \le N_v - 1, 0 \le t \le N_w - 1$), the basis functions $(1-u)v^s w^t$ (for $p = 0$) and $(u+1)v^s w^t$ (for $p = 1$) serve for adjusting the continuity boundary condition for the normal component of the vector $\mathbf{D}$ over sides $u = -1$ and $u = 1$, respectively, of the element (divergence conformity), while the remaining basis functions (for $2 \le p \le N_u$) are zero at the hexahedron sides and serve for improving the current approximation throughout the volume. From (8)–(10), this vector component for the side $u = -1$, for instance, is

$$(D_u)_{\text{norm}} = D_u \sin\theta_{u(v,w)} = D_u(-1,v,w)\frac{(\mathbf{a}_v \times \mathbf{a}_w)\cdot \mathbf{a}_u}{|\mathbf{a}_v \times \mathbf{a}_w||\mathbf{a}_u|}$$
$$= \frac{2}{|\mathbf{a}_v(-1,v,w) \times \mathbf{a}_w(-1,v,w)|} \times \sum_{s=0}^{N_v-1}\sum_{t=0}^{N_w-1} \alpha_{u0st} v^s w^t \tag{11}$$

where D_u denotes the u-component of $\mathbf{D}$ at the side (the v- and w-components of $\mathbf{D}$ are tangential to the side), and $\theta_{u(v,w)}$ the angle between the u parametric line and vw parametric surface at the same point. Since the respective unitary vectors tangential to the side, $\mathbf{a}_v(-1,v,w)$ and $\mathbf{a}_w(-1,v,w)$, are the same for the two adjacent elements sharing the side, the continuity condition between the elements, for $-1 \le v, w \le 1$, can readily (automatically) be enforced, regardless of the adopted geometrical orders, current-expansion orders, or local orientations of the elements. Shown in Fig. 3 is an example of an element (e_1) of the first geometrical order in all directions ($K_u^{e_1} = K_v^{e_1} = K_w^{e_1} = 1, M^{e_1} = 8$) and an element (e_2) of the second geometrical order in all directions ($K_u^{e_1} = K_v^{e_1} = K_w^{e_1} = 2, M^{e_2} = 27$) that are adjacent in the mesh and share a common face. Moreover, the two elements have different current-approximation orders in all respective dimensions ($N_u^{e_1} = 1$, $N_v^{e_1} = 2$, $N_w^{e_1} = 2$ and $N_u^{e_2} = 7$, $N_v^{e_2} = 5$, $N_w^{e_2} = 3$). The continuity of the normal displacement vector component across the common face is imposed by equating the corresponding normal-vector coefficients, α_{u0st} in (11), associated with e_1 and e_2, so that these coefficients are common for the two elements, with additional corrections (sign change) due to possibly different element orientations. For elements with different current-expansion orders,

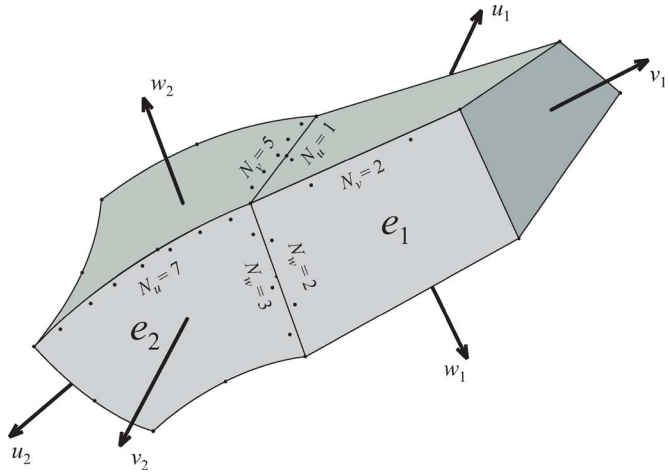

Fig. 3. A connection of two generalized hexahedral elements with different geometrical orders, current-approximation orders, and orientations.

the normal-vector coefficients are matched only up to the lesser of the corresponding orders and are set to zero for the remaining normal-vector basis functions. This order reduction pertains to the common face only and does not influence the expansions throughout the rest of the volumes of the higher order elements. In VIE modeling, the use of bases automatically (for any numerical solution) satisfying the continuity of the normal component of $\mathbf{D}$ at joints of elements in the model actually ensures that theoretically nonexistent surface charges at a boundary between elements across which the properties of the dielectric are continuous functions (e.g., for homogeneous elements made of the same dielectric) cannot be obtained as a consequence of inaccurate numerical solution of a problem. It also enables accurate computing of the surface charge density as $\rho_S = (C_2 - C_1)\mathbf{n}\cdot\mathbf{D}$ ($\mathbf{n}$ directed from element 2 toward element 1) at element interfaces with a discontinuity in ε_e ($C_1 \ne C_2$). Of course, the VIE methodology inherently does not require imposition of any normal-component continuity boundary condition across element interfaces in the model. For example, VIE solutions for $\mathbf{J}$, in (1), as unknown quantity, such as the higher order method in [20], do not impose any continuity across element boundaries and do not seek for nor benefit from the use of divergence-conforming bases; however, these solutions are generally numerically less stable and accurate and require more unknowns than those with the imposition of the $\mathbf{n}\cdot\mathbf{D}$ continuity and the associated bases. Finally, since the vector $\mathbf{D}$ in air is not modeled, the boundary condition for $\mathbf{D}_{\text{norm}}$ on the interface dielectric/air is not enforced automatically but numerically, taking into account the surface charge on the interface.

Note also that the sum limits in (8) that correspond to the variations of a displacement vector component in the directions across that component are by one smaller than the order corresponding to the variation in the other parametric coordinate. This mixed-order arrangement, which ensures equal approximation orders for volume charge densities corresponding to the u-, v-, and w-directed current basis functions, has been found to be a preferable choice for modeling of volume currents in all applications. It enables considerable reductions in the overall number of unknowns, at no expense in terms of the accuracy of current and charge modeling throughout the elements. Note finally that

similar higher order basis functions in the curl-conforming form are used in the FEM analysis [37], as well as that the 2-D (surface) version of the bases is employed in the SIE solution [17].

Finally, what is extremely important, in our VSIE technique for analysis of composite metallic and dielectric radiation/scattering structures, generalized curvilinear quadrilateral elements with 2-D higher order basis functions for SIE modeling of the surface current density $\mathbf{J}_{\mathrm{S}}$ over metallic surfaces are formally treated as degenerate generalized hexahedral elements, in Fig. 1, having the w-dimension suppressed, with the displacement vector $\mathbf{D}$, in (8), or the displacement current density, having only u- and v-components, with the w-component suppressed. In addition, thin metallic wires are formally treated as double-degenerate hexahedra with only the u-component of the vector $\mathbf{D}$ standing for the line current intensity, I, along the generatrices of wires (the reduced-kernel approximation for wires) [23]. This approach is formally implemented in all interactions of volume and surface elements (and wires) and the associated testing and basis functions, to dramatically reduce the number of possible combinations in treatments of elements of different nature in topological analysis of the structure in preprocessing, filling the MoM matrix through multiple levels of integration and packing the MoM generalized impedances and voltages, and field computations in postprocessing.

C. Generalized Galerkin Impedances and Potential Integrals for Double-Higher-Order Hexahedral VIE Elements

In order to determine the unknown coefficients $\{\alpha\}$ in (8), the VSIE system in (5) and (6) is tested by means of the Galerkin method, i.e., using the same functions used for current expansion. The VIE-VIE type of generalized Galerkin impedances (the system matrix elements) corresponding to the volume-current testing and basis functions $\mathbf{f}_m$ and $\mathbf{f}_n$ defined on the mth and nth generalized hexahedral volume elements (V_m and V_n), respectively, in the model are given by [21]

$$Z_{mn}^{\mathrm{vv}} = \int\limits_{V_m} \frac{1}{\varepsilon_{en}} \mathbf{f}_m \cdot \mathbf{f}_n \mathrm{d}V_m + \mathrm{j}\omega \int\limits_{V_m} \mathbf{f}_m \cdot \mathbf{A}_n \mathrm{d}V_m - \int\limits_{V_m} \nabla \cdot \mathbf{f}_m \Phi_n \mathrm{d}V_m + \int\limits_{S_m} \Phi_n \mathbf{f}_m \cdot \mathrm{d}\mathbf{S}_m \quad (12)$$

where $\mathbf{A}_n$ and Φ_n are potentials due to the basis function $\mathbf{f}_n$ and the last two integral terms are obtained expanding $\nabla \cdot (\mathbf{f}_m \Phi_n)$ and applying the divergence theorem, with S_m being the surface of the mth element, oriented outward. Similar expressions hold for VIE-SIE, SIE-VIE, and SIE-SIE generalized Galerkin impedances. To illustrate the procedure for computing these impedances, we consider, without the loss of generality, only the u-components of basis and testing functions. Furthermore, we consider the functions in the following simplified form:

$$\mathbf{f} = \mathbf{f}_{upst} = \frac{u^p v^s w^t}{\Im} \frac{\partial \mathbf{r}}{\partial u} \quad [Q_p(u) = u^p]. \quad (13)$$

The generalized Galerkin impedances corresponding to the complete, divergence-conforming, basis functions in (9) can be obtained as a linear combination of those corresponding to the simplified, three-dimensional power functions in (13).

Upon substituting (13) and (7), the second integral term in (12) corresponding to the testing function defined by indices p_m, s_m, and t_m on the mth hexahedron and the basis function defined by indices p_n, s_n, and t_n on the nth hexahedron in the model becomes

$$\begin{aligned}
&\mathrm{j}\omega \int\limits_{V_m} \mathbf{f}_m \cdot \mathbf{A}_n \mathrm{d}V_m \\
&\quad = -\omega^2 \mu_0 C_n \int\limits_{-1}^{1}\int\limits_{-1}^{1}\int\limits_{-1}^{1}\int\limits_{-1}^{1}\int\limits_{-1}^{1}\int\limits_{-1}^{1} \mathbf{f}_m(p_m, s_m, t_m) \\
&\qquad \cdot \mathbf{f}_n(p_n, s_n, t_n) \\
&\qquad \times g(R) \Im_n \Im_m \mathrm{d}u_n \mathrm{d}v_n \mathrm{d}w_n \mathrm{d}u_m \mathrm{d}v_m \mathrm{d}w_m \\
&\quad = -\omega^2 \mu_0 C_n \sum_{i_m=1}^{K_u^{(m)}} \sum_{j_m=0}^{K_v^{(m)}} \sum_{k_m=0}^{K_w^{(m)}} \sum_{i_n=1}^{K_u^{(n)}} \sum_{j_n=0}^{K_v^{(n)}} \sum_{k_n=0}^{K_w^{(n)}} i_m i_n \\
&\qquad \times \left(\mathbf{r}_{i_m j_m k_m}^{(m)} \cdot \mathbf{r}_{i_n j_n k_n}^{(n)} \right) \\
&\qquad \times \int\limits_{-1}^{1}\int\limits_{-1}^{1}\int\limits_{-1}^{1}\int\limits_{-1}^{1}\int\limits_{-1}^{1}\int\limits_{-1}^{1} u_m^{p_m+i_m-1} v_m^{s_m+j_m} w_m^{t_m+k_m} \\
&\qquad \times u_n^{p_n+i_n-1} v_n^{s_n+j_n} w_n^{t_n+k_n} g(R) \\
&\qquad \times \mathrm{d}u_n \mathrm{d}v_n \mathrm{d}w_n \mathrm{d}u_m \mathrm{d}v_m \mathrm{d}w_m \\
&p_m = 0,\, 1, \ldots, N_u^{(m)}, s_m = 0,\, 1, \ldots, N_v^{(m)} \\
&t_m = 0,\, 1, \ldots, N_w^{(m)} \\
&p_n = 0,\, 1, \ldots, N_u^{(n)}, s_n = 0,\, 1, \ldots, N_v^{(n)} \\
&t_n = 0,\, 1, \ldots, N_w^{(n)}
\end{aligned} \quad (14)$$

where $K_u^{(m)}$, $K_v^{(m)}$, and $K_w^{(m)}$ are the geometrical orders and $N_u^{(m)}$, $N_v^{(m)}$, and $N_w^{(m)}$ the current approximation orders along the u-, v-, and w-coordinate, respectively, and $\mathbf{r}_{ijk}^{(m)}$ are the geometrical vector coefficients in the polynomial expansion of the mth hexahedron, while $K_u^{(n)}$, $K_v^{(n)}$, $K_w^{(n)}$, $N_u^{(n)}$, $N_v^{(n)}$, $N_w^{(n)}$, and $\mathbf{r}_{ijk}^{(n)}$ are the corresponding parameters for the nth hexahedron, which is assumed, for simplicity, to be filled with a homogeneous dielectric of contrast C_n. The source-to-field distance R is computed as

$$R = |\mathbf{r}_m(u_m, v_m, w_m) - \mathbf{r}_n(u_n, v_n, w_n)|. \quad (15)$$

Similarly, the third integral term in (12) is transformed to

$$\begin{aligned}
&-\int\limits_{V_m} \nabla \cdot \mathbf{f}_m \Phi_n \mathrm{d}V_m \\
&\quad = \frac{C_n}{\varepsilon_0} \int\limits_{-1}^{1}\int\limits_{-1}^{1}\int\limits_{-1}^{1}\int\limits_{-1}^{1}\int\limits_{-1}^{1}\int\limits_{-1}^{1} p_m p_n u_m^{p_m-1} \\
&\qquad \times v_m^{s_m} w_m^{t_m} u_n^{p_n-1} v_n^{s_n} w_n^{t_n} g(R) \\
&\qquad \times \mathrm{d}u_n \mathrm{d}v_n \mathrm{d}w_n \mathrm{d}u_m \mathrm{d}v_m \mathrm{d}w_m \\
&\qquad - \frac{C_n}{\varepsilon_0} \int\limits_{-1}^{1}\int\limits_{-1}^{1}\int\limits_{-1}^{1}\int\limits_{-1}^{1}\int\limits_{-1}^{1} p_m u_m^{p_m-1} \\
&\qquad \times v_m^{s_m} w_m^{t_m} u_n^{p_n} v_n^{s_n} w_n^{t_n} g(R) \\
&\qquad \times \mathrm{d}v_n \mathrm{d}w_n \mathrm{d}u_m \mathrm{d}v_m \mathrm{d}w_m |_{u_n=1}
\end{aligned}$$

$$+\frac{C_n}{\varepsilon_0}\int_{-1}^{1}\int_{-1}^{1}\int_{-1}^{1}\int_{-1}^{1}\int_{-1}^{1} p_m u_m^{p_m-1} v_m^{s_m} w_m^{t_m} u_n^{p_n} \times v_n^{s_n} w_n^{t_n} g(R) \times \mathrm{d}v_n \mathrm{d}w_n \mathrm{d}u_m \mathrm{d}v_m \mathrm{d}w_m|_{u_n=-1} \quad (16)$$

where, according to (3), the first integral term in this newly developed expression corresponds to the portion of the potential Φ_n due to the volume charges inside the nth hexahedron, while the second and third terms are associated with the contributions to Φ_n due to the surface charges on the sides of this hexahedron defined by $u_n = 1$ and $u_n = -1$, respectively. Moreover, in packing the generalized Galerkin impedances for divergence-conforming basis functions in (9), the latter two terms are taken into account (and are actually computed in the first place) only for basis functions $(1-u_n)v_n^{s_n}w_n^{t_n}$ (for $p_n = 0$) and $(u_n+1)v_n^{s_n}w_n^{t_n}$ (for $p_n = 1$), respectively, and only if the dielectric properties vary across the respective side of the hexahedron (e.g., for sides belonging to dielectric-air interfaces in the model). Analogous final expressions are obtained for the remaining two terms of the VIE-VIE generalized Galerkin impedance. Of crucial importance is that all these impedance terms, as well as VIE-SIE, SIE-VIE, and SIE-SIE ones, for basis/testing functions in (13), as well as for those in (9), can be represented as linear combinations of 3-D/3-D basic Galerkin potential integrals with only simple power functions and Green's function as integrands

$$S(h_m, l_m, q_m, h_n, l_n, q_n) = \int_{-1}^{1}\int_{-1}^{1}\int_{-1}^{1} u_m^{h_m} v_m^{l_m} w_m^{q_m} P(h_n, l_n, q_n) \times \mathrm{d}u_m \mathrm{d}v_m \mathrm{d}w_m \quad (17)$$

where P are the 3-D basic potential integrals, evaluated as

$$P(h_n, l_n, q_n) = \int_{-1}^{1}\int_{-1}^{1}\int_{-1}^{1} u_n^{h_n} v_n^{l_n} w_n^{q_n} g(R) \mathrm{d}u_n \mathrm{d}v_n \mathrm{d}w_n \quad (18)$$

and the corresponding 3-D/2-D, 2-D/3-D, and 2-D/2-D Galerkin integrals. This is extremely important because Galerkin integrals with only simple power functions and Green's function as integrands enable rapid and accurate recursive and nonredundant procedures for evaluation of the generalized MoM impedances. Equally important is the fact that there is no need for computing the corresponding field integrals, which is not the case in SIE analysis of dielectric and composite metallic/dielectric structures, where the computation of hyper-singular field integrals is needed to find the electric and magnetic fields in coupled electric/magnetic field integral equations (EFIE/MFIE) with electric and magnetic surface currents as unknowns [17].

In specific, efficient algorithms for recursive construction of the generalized Galerkin impedances and the VSIE system matrix are developed in order to avoid redundant operations related to the indices i, j, and k for geometrical representations and p, s, and t for current expansions within the impedances, as well as the summation indices in the Gauss-Legendre integration formulas used for numerical integration, for any pair, m and n, of hexahedral elements in the model. In addition, since the coordinates u, v and w, as well as the corresponding indices, in the integrals S in (17) and (18), and analogously for other integrals in the technique, are cyclic, the same sequence of the S integrals (for all the required values of the subscripts h_m, l_m, q_m, h_n, l_n, and q_n) for a given pair of hexahedra can be used also for the evaluation of the generalized impedances relating to the v- and w-components of the vector $\mathbf{D}$ in the two hexahedra (note that there are nine combinations for the impedances corresponding to the three components of the testing and basis vector functions in the two elements). In addition, the same sequence of the S integrals can be used both in the impedances in (14) and in the 3-D/3-D part of the impedances in (16). So, for any hexahedron pair in the model, first and only once the entire sequence of the basic Galerkin integrals S is evaluated, and these integrals are then introduced (packed) into all impedances containing them. In the next level of packing, the impedances for basis/testing functions in (13) are recursively and nonredundantly combined into the final Galerkin impedances for functions in (9).

A rapid and accurate combined numerical/analytical method is developed for the integration over curved higher order generalized hexahedral elements, for the P integrals in (18). When the distance R in (15) is relatively small or zero, the procedure of extracting the singularity is performed, which consists of analytical integration of a principal singular part of the integrand over a (generally not rectangular) parallelepiped whose parametric description is close to that of the generalized hexahedron in the vicinity of the singular point, and numerical integration of the rest using Gauss-Legendre quadrature formulas. The sides of the parallelepiped that corresponds to the generalized hexahedron specified in (7) are obtained by translating the straight segments A_1A_2, B_1B_2, and C_1C_2 shown in Fig. 4, where these segments, in turn, are obtained differentiating the curves defined by $\mathbf{r}(u, v_0, w_0)$, $\mathbf{r}(u_0, v, w_0)$, and $\mathbf{r}(u_0, v_0, w)$ at the point (u_0, v_0, w_0). In other words, the parallelepiped is defined by the unitary vectors $\mathbf{a}_u$, $\mathbf{a}_v$, and $\mathbf{a}_w$ of the generalized hexahedron, (10), at the singular point, and hence its parametric equation:

$$\mathbf{r}_\mathrm{p}(u,v,w) = \mathbf{r}_\mathrm{c} + \mathbf{a}_{u0}(u-u_0) + \mathbf{a}_{v0}(v-v_0) + \mathbf{a}_{w0}(w-w_0) \quad -1 \le u, v, w \le 1 \quad (19)$$

where u_0, v_0, and w_0 are the coordinates of the singular point and $\mathbf{r}_\mathrm{c} = \mathbf{r}(u_0, v_0, w_0)$, $\mathbf{a}_{u0} = \mathbf{a}_u(u_0, v_0, w_0)$, $\mathbf{a}_{v0} = \mathbf{a}_v(u_0, v_0, w_0)$, and $\mathbf{a}_{w0} = \mathbf{a}_w(u_0, v_0, w_0)$. For u close to u_0, v close to v_0, and w close to w_0, the point $M(u, v, w)$ of the curved hexahedron coincides with or is very close to the point $M_\mathrm{p}(u, v, w)$ of the parallelepiped. Therefore, in extracting the singularity in the P integrals, we subtract and add a term of the form $1/R_\mathrm{p}$ (instead of $1/R$), where

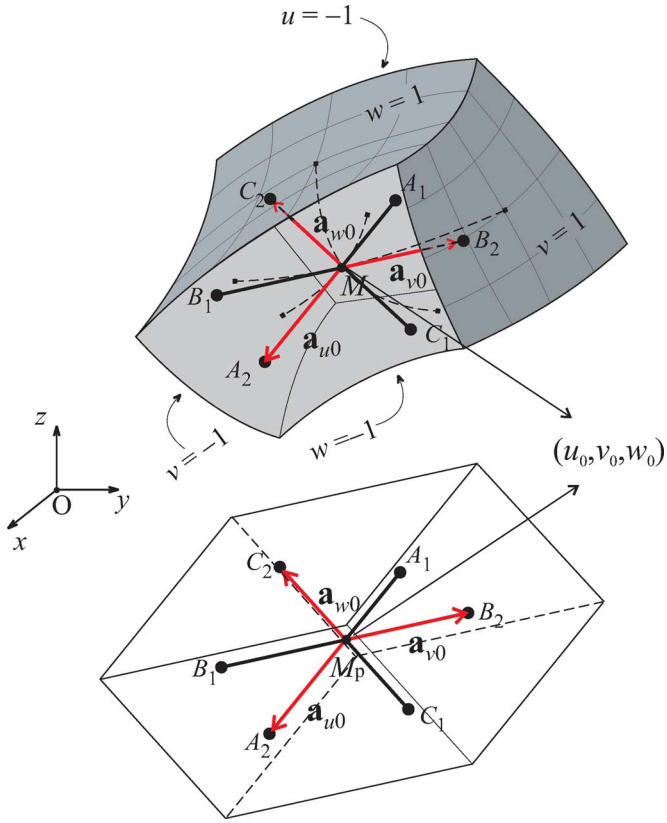

Fig. 4. Finding the parallelepiped whose parametric description is close to that of a curved higher order generalized hexahedral VIE element in the vicinity of the singular point (u_0, v_0, w_0) (note that the case presented here is for $u_0 = v_0 = w_0 = 0$)—for the singularity extraction procedure in (20) to solve the 3-D basic potential integrals over curved hexahedra.

$R_{\rm p} = \mathbf{r}_{\rm c} - \mathbf{r}_{\rm p}(u, v, w)$ is the source-to-field distance for integration throughout the volume of the parallelepiped [22]

$$P(h,l,q) = \int_{-1}^{1}\int_{-1}^{1}\int_{-1}^{1} \left(u^h\, v^l\, w^q\, g(R) - u_0^h v_0^l w_0^q \cos(\beta_0 d)\frac{1}{4\pi R_{\rm p}} \right) {\rm d}u{\rm d}v{\rm d}w + \frac{u_0^h v_0^l w_0^q \cos(\beta_0 d)}{4\pi} \int_{-1}^{1}\int_{-1}^{1}\int_{-1}^{1} \frac{1}{R_{\rm p}} {\rm d}u{\rm d}v{\rm d}w \tag{20}$$

with d being determined as $d = R_{\min}$ [of course, for the observation (field) point inside the generalized hexahedron or on its surface, $d = 0$]. In (20), the first integral is well behaved in the vicinity of the point (u_0, v_0, w_0) and can be rather accurately integrated numerically, over the domain $-1 \le u, v, w \le 1$, which represents the domain of both the curved hexahedron and the parallelepiped. However, to further enhance the accuracy of the numerical integration, we subdivide this domain into a number of integration subdomains by means of coordinate surfaces $u = u_0$, $v = v_0$, and $w = w_0$, respectively. Note that this technique remains practically the same when P is a near-singular integral, namely, when the observation point is outside the generalized hexahedron but very close to its surface.

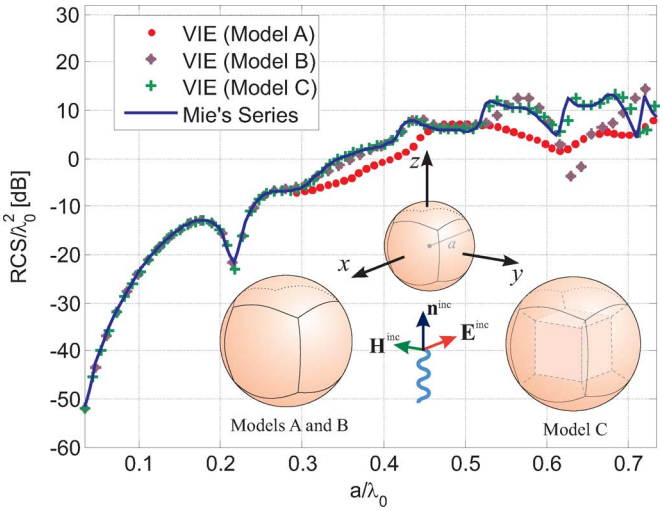

Fig. 5. Normalized monostatic radar cross section (RCS) of a dielectric ($\varepsilon_{\rm r} = 4$) sphere (λ_0 is the free-space wavelength): comparison of numerical solutions obtained by three double-higher-order VIE models (A, B, and C) with the analytical solution in the form of Mie's series.

III. Numerical Results and Discussion

Note that a direct solver is utilized for the solution of the MoM-VSIE system of equations in all examples.

A. Homogeneous Dielectric Scatterer

As the first example of curved dielectric structures, consider a lossless homogeneous spherical dielectric scatterer of radius a, shown in the top inset of Fig. 5. Relative permittivity of the dielectric is $\varepsilon_{\rm r} = 4$. Fig. 5 presents the monostatic radar cross section (RCS) of the scatterer, normalized to λ_0^2, as a function of a/λ_0, λ_0 being the free-space wavelength. The numerical results obtained by three higher order VIE solutions, with the sphere modeled using (A) one curved hexahedron with geometrical orders $K_u = K_v = K_w = 2$ [Fig. 2(b)], orders $N_u = N_v = N_w = 4$ for the polynomial approximation of the displacement vector in the element, and only $N_{\rm unkn}^{\rm VIE} = 240$ unknowns (without the use of symmetry), (B) one hexahedron with $K_u = K_v = K_w = 4$ and $N_u = N_v = N_w = 4$, and (C) seven large elements, with the central element in the form of a cube ($K_u = K_v = K_w = 1$) and six cushion-like curved hexahedral elements ($K_u = K_v = K_w = 2$) attached to the cube sides (the mesh is shown in the lower right inset of Fig. 5) and $N_u = N_v = N_w = 6$ in all of the elements ($N_{\rm unkn}^{\rm VIE} = 5,004$), are compared with the analytical solution in the form of Mie's series. Note that the single-element models A and B (lower left inset of Fig. 5) are literally entire-domain curved CEM models. Note also that the model B is aimed to illustrate the solution behavior when the geometrical approximation is improved, while the principal purpose of the solution C is to evaluate an hp-refinement of the model, with both the number of elements increased (h-refinement) and the current approximation in the elements enhanced (p-refinement). We observe, in Fig. 5, that, as compared to the exact solution (Mie's

TABLE I
RCS SOLUTION ERROR AND MOM MATRIX CONDITION NUMBER FOR A SINGLE-ELEMENT SPHERE MODEL VERSUS ELEMENT GEOMETRICAL ORDERS

$K_u = K_v = K_w$	Error	Condition number
2	28%	7903.98
3	11%	8571.01
4	0.3%	3909.71

TABLE II
RCS ERROR AND CONDITION NUMBER FOR A SINGLE-ELEMENT SPHERE MODEL VERSUS CURRENT EXPANSION ORDERS

$N_u = N_v = N_w$	Error	Condition number
4	28%	7903.98
5	4.7%	689578.19
6	4.1%	56342600.00

series), models A and B perform well up to the frequency at which $a/\lambda_{\rm d} = 0.6$ and 1.02, respectively, where $\lambda_{\rm d} = \lambda_0/\sqrt{\varepsilon_{\rm r}}$ is the wavelength in the dielectric, which demonstrates a dramatic improvement of results when using geometrical modeling of the 4th order instead of the 2nd order geometrical modeling. In the latter case, when $a/\lambda_{\rm d} = 1.02$, the central dimension of the single hexahedral element used to model the sphere is about $e = 2a = 2.04\lambda_{\rm d}$ (sphere diameter), which indicates that the proposed double-higher-order VIE technique allows using curved elements that are as large as $e \approx 2\lambda_{\rm d}$ across. We also observe a very significant improvement of results employing the *hp*-refined model C, which gives a good agreement with Mie's series solution up to the frequency at which $a/\lambda_{\rm d} = 1.38$. The largest dimension of the hexahedra in this model is approximately $e = 1.6a = 2.21\lambda_{\rm d}$ for cushion-like hexahedra, while the size of the cubical element in the middle amounts to $e = 1.15\lambda_{\rm d}$. In addition, note that among the three models of the sphere, models A and B have geometrical degeneracy around the corners of the hexahedral elements, which reflects on the current expansion through the Jacobian and influences the accuracy of the solution. Note also that computation of the Jacobian is actually not needed except in the first integral term in (12), since the Jacobians cancel out in final expressions for all other integral terms, as can be seen in (14) and (16).

As an additional evaluation of convergence properties of the double higher-order VIE analysis, Table I gives the percentage error of RCS computation relative to the Mie's series solution, $\text{error} = |(\text{RCS}^{\text{Mie}} - \text{RCS}^{\text{VIE}})/\text{RCS}^{\text{Mie}}| \cdot 100\%$ and condition number of the MoM matrix for the sphere of diameter $d = 1.24\lambda_{\rm d}$ modeled by a single curved hexahedron whose geometrical orders are varied from $K_u = K_v = K_w = 2$ to $K_u = K_v = K_w = 4$, while keeping the current approximation orders constant, $N_u = N_v = N_w = 4$.

Table II shows the error and condition number for constant geometrical orders, $K_u = K_v = K_w = 2$, and current expansion orders varied from $N_u = N_v = N_w = 4$ to $N_u = N_v = N_w = 6$. We observe in Tables I and II an excellent convergence of the VIE method with increasing both geometrical and current-approximation orders. Also, as expected, the condition number is almost unaffected by the geometrical orders, while it rapidly increases with increasing the orders of basis functions.

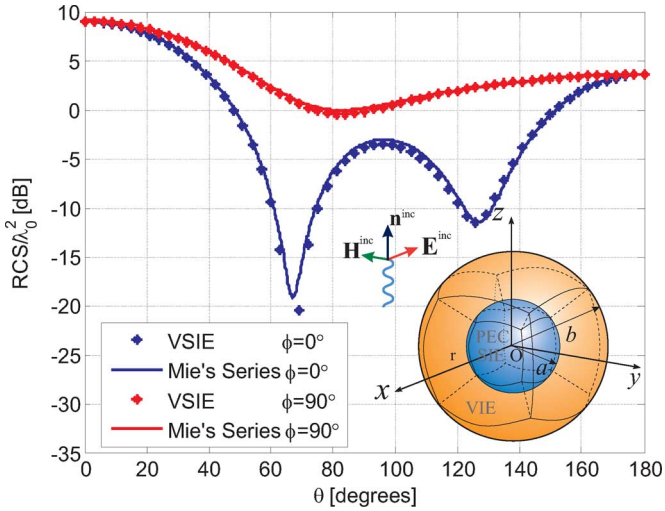

Fig. 6. Normalized bistatic radar cross section in two characteristic planes of a dielectrically coated PEC sphere ($\varepsilon_{\rm r} = 4$, $2a = b = 10$ cm, $f = 1$ GHz): comparison of the double-higher-order VSIE results with the exact Mie's series solution; figure inset shows a higher order VSIE mesh of the scatterer using six large cushion-like conformal hexahedral VIE elements and six curved quadrilateral SIE patches.

However, the orthogonality and conditioning properties of the simplest hierarchical divergence-conforming polynomial vector basis functions, in (9), can be improved as in [29], [40], [41], for instance, and this is needed when iterative solvers are used.

B. Composite Metallic/Dielectric Structure

As an example of composite metallic/dielectric structures, that also possess curvature, consider a dielectrically coated PEC sphere excited by a plane wave, of frequency $f = 1$ GHz, as shown in the inset of Fig. 6. The radii of the PEC sphere and the coated sphere are $a = 5$ cm and $b = 10$ cm, respectively, and the relative permittivity of the dielectric of the coating is $\varepsilon_{\rm r} = 4$. The coating is modeled using only six large cushion-like conformal hexahedral VIE elements with $K_u = K_v = K_w = 2$ and $N_u = N_v = N_w = 6$, and the PEC surface is modeled by six curved quadrilateral SIE patches with $K_u = K_v = 2$ and $N_u = N_v = 6$, as depicted in the figure inset, resulting in a total of $N_{\rm unkn}^{\rm VSIE} = 4,824$ unknowns. The size of the volume and surface elements in the model ranges between $0.53\lambda_{\rm d} \leq e \leq 1.06\lambda_{\rm d}$. Fig. 6 shows the computed bistatic RCS of the scatterer in two characteristic planes, where an excellent agreement of the double-higher-order VSIE results with the exact solution in the form of Mie's series is observed (the average absolute RCS errors, over all θ angles, are 0.45 dB and 0.13 dB in planes $\phi = 0°$ and $\phi = 90°$, respectively).

C. Continuously Inhomogeneous Dielectric Scatterer

As an example of inhomogeneous dielectric structures, that are also curved, consider a continuously inhomogeneous dielectric spherical scatterer of radius $a = 1$ m and a linear radial variation of relative permittivity from $\varepsilon_{\rm r} = 1$ at the surface to $\varepsilon_{\rm r} = 6$ at the center of the sphere, as depicted in the inset of Fig. 7. The scatterer is situated in free space and illuminated by a uniform plane wave. The sphere is modeled by 7 curvilinear hexahedral elements of the fourth geometrical order

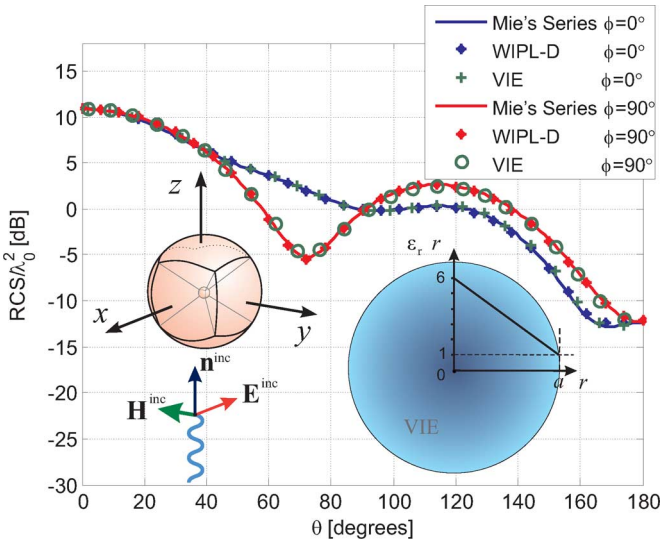

Fig. 7. Normalized bistatic radar cross section in two characteristic planes of a continuously inhomogeneous dielectric sphere (shown in the inset): comparison of the double-higher-order inhomogeneous-VIE solution and WIPL-D results for a five-layer piecewise homogeneous SIE model, as well as the Mie series solution for the five-layer model.

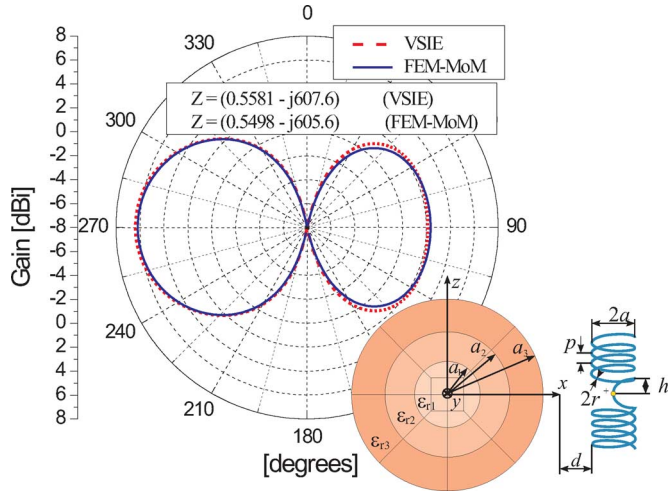

Fig. 8. Analysis of an eight-turn helical dipole antenna ($2a = 5$ mm, $p = 1.25$ mm, $h = 1.77$ mm, $2r = 0.2$ mm, $d = 5$ mm, $f = 900$ MHz) near an inhomogeneous, three-layer, dielectric sphere ($a_1 = 4$ cm, $a_2 = 7$ cm, $a_3 = 10$ cm, $\varepsilon_{r1} = 2$, $\varepsilon_{r2} = 4$, $\varepsilon_{r3} = 6$) [42], modeled by 8 cubical and 72 curvilinear hexahedral VIE elements (figure inset shows a cross section of the VIE model): comparison of results for the radiation (gain) pattern of the antenna in the $\phi = 0°$ plane and for the antenna input impedance obtained by the double-higher-order VSIE method with reference FEM-MoM results [42].

$(K_u = K_v = K_w = 4)$. In specific, the central sphere (of radius $a/30$) is modeled using a single VIE element, and a layer of six inhomogeneous cushion-like VIE elements are attached to the corresponding sides of the central element. The current approximation orders are $N_u = N_v = N_w = 1$ for the small central element and $N_u = N_v = N_w = 4$ for all the "cushions," which results in a total of $N_{\text{unkn}}^{\text{VIE}} = 1,350$ unknowns. The VIE solution for the continuously inhomogeneous model is compared with a SIE solution for the approximately equivalent piecewise homogeneous layered model consisting of five concentric dielectric layers defined by radii $a_1 = 0.2$ m, $a_2 = 0.4$ m, $a_3 = 0.6$ m, $a_4 = 0.8$ m, and $a_5 = 1$ m, with relative permittivities $\varepsilon_{\text{r1}} = 5.875$, $\varepsilon_{\text{r2}} = 5.16$, $\varepsilon_{\text{r3}} = 3.97$, $\varepsilon_{\text{r4}} = 2.78$, and $\varepsilon_{\text{r5}} = 1.59$, respectively. The layered sphere is modeled in WIPL-D (commercial higher order SIE code [2]) by 678 bilinear quadrilateral elements with $N_u = N_v = 1$ and the total count of $N_{\text{unkn}}^{\text{SIE}} = 2,712$ unknowns. Shown in Fig. 7 is the simulated bistatic RCS of the scatterer in two characteristic planes at $f = 150$ MHz, where we observe an excellent agreement of the double-higher-order inhomogeneous-VIE, layered-SIE, and layered-Mie-series solutions. The average absolute RCS differences (over all θ angles) between the VIE solution for the continuously inhomogeneous model and the Mie-series solution for the five-layer model are 0.1 dB and 0.13 dB in planes $\phi = 0°$ and $\phi = 90°$, respectively, while the corresponding differences between the WIPL-D and Mie-series solutions for the layered model amount to 0.12 dB and 0.1 dB.

D. Wire Antenna Coupled to an Inhomogeneous Dielectric Body

As an antenna example, consider an eight-turn helical dipole antenna near an inhomogeneous dielectric sphere composed of three concentric dielectric layers, as shown in the inset of Fig. 8 [42]. The sphere is modeled by 8 cubical $(K_u = K_v = K_w = 1)$ and 72 curvilinear triquadratic $(K_u = K_v = K_w = 2)$ hexahedral VIE elements, as indicated in Fig. 8, with the orders N_u, N_v, and N_w varied from 2 to 3 for different elements and in different directions, and the helical antenna is modeled by 72 straight $(K_u = 1)$ SIE wire segments [42] with $N_u = 2$ for each of the segments, which results in a total of $N_{\text{unkn}}^{\text{VSIE}} = 6,995$ unknowns. Shown in Fig. 8 is the simulated radiation (gain) pattern of the antenna in the $\phi = 0°$ plane, as well as the simulation results for the antenna impedance, at $f = 900$ MHz, obtained by the proposed higher order VSIE technique and by the higher order FEM-MoM technique $(N_{\text{unkn}}^{\text{FEM-MoM}} = 7,447)$ [42], respectively, and an excellent agreement of the two sets of results is observed, for both the far field (the average absolute gain difference in the entire $\phi = 0°$ plane is 0.28 dB) and the impedance of the antenna, with the VSIE and FEM-MoM solutions implementing identical volumetric geometrical models of the layered sphere but, of course, discretizing very different equations throughout its volume.

E. Finite Array of Dielectric Scatterers (PBG Waveguide)

As the next example, consider an infrared (IR) photonic band gap (PBG) waveguide realized, as a combination of PBG waveguide concepts proposed in [43] and [44], as a pattern of 72 circular dielectric (GaAs) rods, with $\varepsilon_{\text{r}} = 11.4$, in an air background shown in Fig. 9(a). The height of each cylinder is $h = 1.11$ μm, diameter is $2a = 288$ nm, and the distance between the axes of adjacent cylinders is $d = 750$ nm. The array of rods is situated between two PEC plates of size 4.8×8.5 μm, perpendicular to the cylinder axes. The distance between the plates is $D = 1.6$ μm, and they are positioned symmetrically in all directions with respect to the PBG array. The structure is excited by a $l = 674$ nm long wire dipole at its edge [Fig. 9(a)], with the dipole being parallel to the axes of cylinders. In the double-higher-order VSIE model, each cylinder is modeled by a single curved hexahedral volume element with $K_u = K_v = K_w = 2$ and $N_u = N_v = N_w = 3$, as depicted in Fig. 9(b), which yields a total count of $N_{\text{unkn}}^{\text{VSIE}} = 7,965$ unknowns (with

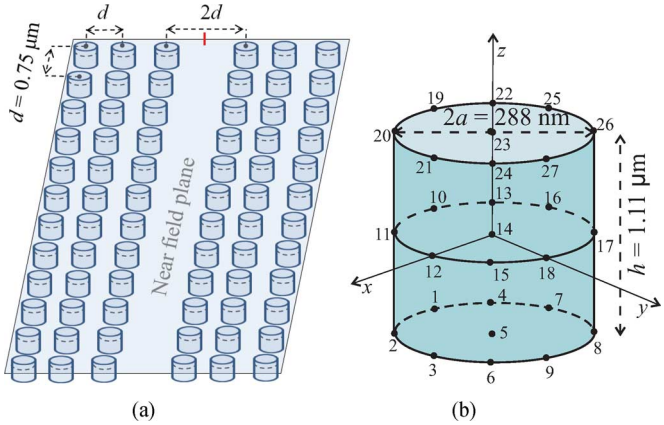

Fig. 9. (a) IR PBG waveguide realized as a pattern of circular dielectric ($\varepsilon_r = 11.4$) rods between two PEC plates (plates not shown) in an air background (the structure is excited by a wire dipole at its edge) and (b) modeling of each cylinder by a single curved hexahedral VIE element of the second geometrical orders.

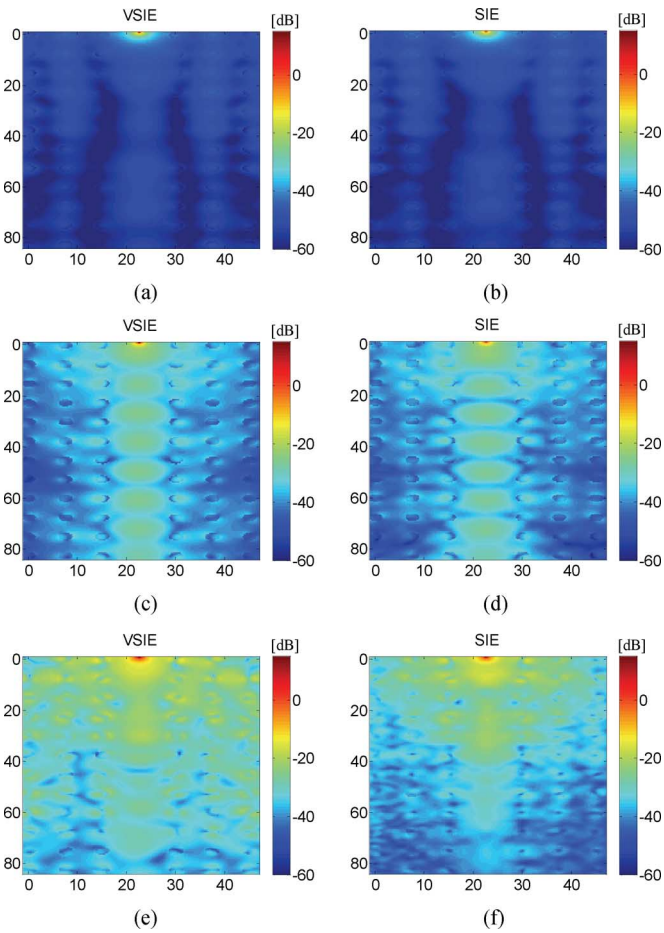

Fig. 10. Magnitude of the near electric field of the PBG structure in Fig. 10(a) computed, in the plane indicated in Fig. 10(a), at frequencies (a)–(b) $f_1 = 120$ THz, (c)–(d) $f_2 = 175$ THz, and (e)–(f) $f_3 = 220$ THz, by (a), (c), (e) the double-higher-order VSIE technique [based on the model of cylinders shown in Fig. 10(b)] and by (b), (d), (f) the double-higher-order SIE technique [17].

no use of symmetry), including the SIE unknowns for modeling the wire dipole and the PEC plates. The near-field distributions calculated in the plane cutting across the dielectric rods at 2/3 of their height, perpendicularly to their axes [this plane is sketched in Fig. 10(a)], at frequencies $f_1 = 120$ THz,

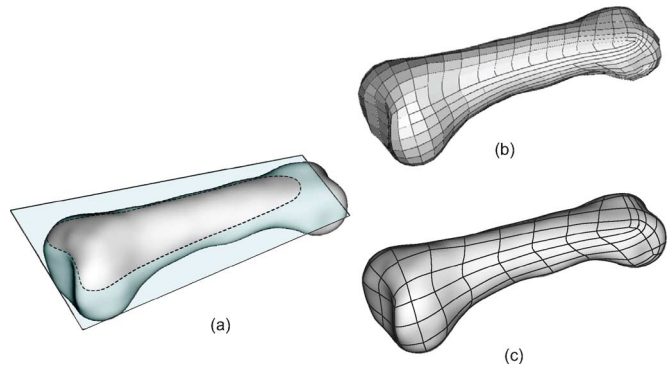

Fig. 11. VIE modeling of a human bone ($\varepsilon_r = 11.38, \sigma = 0.39$): (a) bone geometry, (b) trilinear VIE model, and (c) triquadratic curved VIE model.

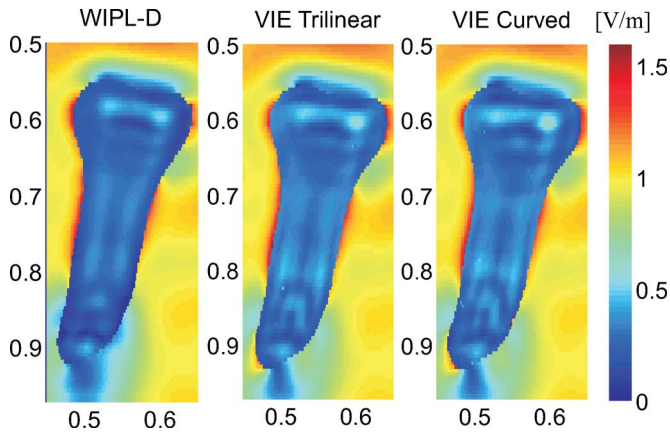

Fig. 12. Magnitude of the electric field in the plane indicated in Fig. 11(a) near or inside a bone model excited by a plane wave with a normal incidence to the plane at $f = 2.5$ GHz: comparison of VIE results obtained using models in Fig. 11(b) and (c) and a fully hp-refined WIPL-D reference solution.

$f_2 = 175$ THz, and $f_3 = 220$ THz, respectively, are shown in Fig. 10, where PBG effects are clearly observed. Field plots in Figs. 10(a) and (b) show no propagation through the structure at the frequency f_1 (stop band of the waveguide within the stop band of the PBG lattice), Figs. 10(c) and (d) depict waveguide propagation at the frequency f_2 (waveguide pass band within the PBG stop band), while the plots in Figs. 10(e) and (f) demonstrate unobstructed propagation through the PBG structure at the frequency f_3 (inside the pass band of the PBG lattice). Moreover, at all frequencies, the double-higher-order VSIE solutions [Figs. 10(a), (c), and (e)] are compared to the results [in Figs. 10(b), (d), and (f)] obtained by the double-higher-order SIE technique [17], with the surface of each cylinder modeled by six curved quadrilateral patches with $K_u = K_v = 2$ and $N_u = N_v = 3$ ($N_{\text{unkn}}^{\text{SIE}} = 15,741$). A good agreement of the two sets of numerical results is observed.

F. Human Bone Model

As an example of curved, geometrically complex dielectric objects, consider a human bone model, shown in Fig. 11(a), illuminated by a plane wave at a frequency $f = 2.5$ GHz. This is also an example of bodies with high electric contrast and losses, namely, the bone permittivity and conductivity are $\varepsilon_r = 11.38$ and $\sigma = 0.39$ S/m [45]. The electrical dimensions of the bone are $5.4518\lambda_d \times 11.5947\lambda_d \times 4.3303\lambda_d$. The results obtained by a trilinear ($K_u = K_v = K_w = 1$) 1,024-element VIE model,

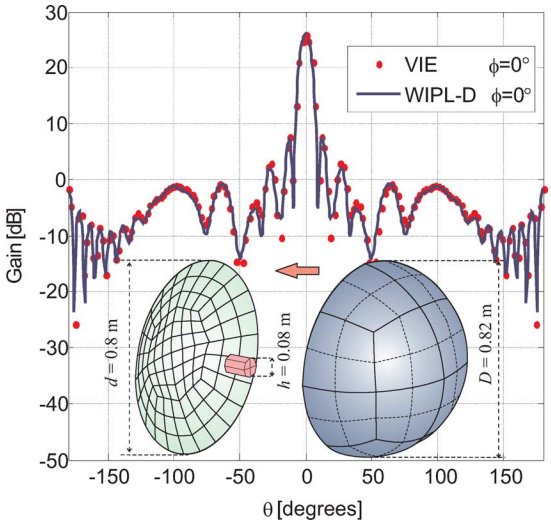

Fig. 13. Analysis of a parabolic satellite dish antenna excited by a cylindrical waveguide section ($f = 3$ GHz) and covered by a hemispherical dielectric ($\varepsilon_{\rm r} = 2.5$) radome (6-mm thick): comparison of results for the radiation pattern (gain) of the antenna in the $\phi = 0^\circ$ plane obtained by the double-higher-order VSIE method (model with 48 curved hexahedral VIE elements, 120 curved quadrilateral SIE patches, and two SIE wire segments) with reference WIPL-D pure-SIE results.

shown in Fig. 11(b), with $N_u = N_v = N_w = 2$, and a triquadratic ($K_u = K_v = K_w = 2$) curved 128-element VIE model, shown in Fig. 11(c), with $N_u = N_v = N_w = 3$, are compared with a fully hp-refined WIPL-D reference solution. Note that the average dimensions of elements in the trilinear and triquadratic models are $e = 0.73\lambda_{\rm d}$ and $e = 1.45\lambda_{\rm d}$, respectively. Fig. 12 shows the near (internal or external) total electric field computed in the plane indicated in Fig. 11(a). We observe a good agreement between the two higher order VIE solutions and the reference solution, with a large saving in the number of unknowns, $N_{\rm unkn}^{\rm VIE} = 11,088$ instead of $N_{\rm unkn}^{\rm VIE} = 25,856$, in favor of the model with curved VIE elements.

G. Satellite Dish Antenna With a Dielectric Radome

As the final example, consider a satellite antenna with a parabolic dish reflector, excited by a cylindrical waveguide section of diameter $h = 0.08$ m and length $l = 0.1$ m, and covered by a hemispherical dielectric radome depicted in the inset of Fig. 13. The reflector dish opening and the radome surface diameters are $d = 0.8$ m and $D = 0.82$ m respectively. The radome is 6 mm thick and its permittivity is $\varepsilon_{\rm r} = 2.5$. The operating frequency is $f = 3$ GHz, and $D = 8.2\lambda_0 = 13.0\lambda_{\rm d}$. The VSIE model consists of 170 elements, namely, 48 hexahedral VIE elements with $K_u = K_v = K_w = 2$, $N_u = 1$, and $N_v = N_w = 4$, 120 quadrilateral SIE patches with $K_u = K_v = 1$ and $N_u = N_v = 4$, and two SIE wire segments with $K_u = 1$ and $N_u = 3$, and resulting in a total of $N_{\rm unkn}^{\rm VSIE} = 6,933$ unknowns. More specifically, the VIE radome model is a layer of 48 thin volumetric blocks, with maximal dimensions amounting to $e = 2.34\lambda_{\rm d}$ and different current approximation orders in radial direction ($N_u = 1$) and directions tangential to the radome surface ($N_v = N_w = 4$). The radiation (gain) pattern of the antenna in the $\phi = 0^\circ$ plane computed by the VSIE is compared in Fig. 13 with the pure SIE solution by WIPL-D, which requires $N_{\rm unkn}^{\rm SIE} = 23,908$ unknowns, and we observe an excellent agreement of the two sets of results.

IV. Conclusion

This paper has proposed a double-higher-order large-domain Galerkin-type method of moments for modeling of composite wire-plate-dielectric radiation/scattering structures. The method is based on the volume integral equation approach for dielectric parts and the surface integral equation approach for metallic parts of the composite structure. It employs Lagrange-type interpolation generalized hexahedra and quadrilaterals of arbitrary geometrical-mapping orders for the approximation of geometry and hierarchical divergence-conforming polynomial vector basis functions of arbitrary expansion orders for the approximation of currents within the elements. The results obtained by the double-higher-order VSIE method have been validated against the analytical solutions and the numerical results obtained by the double-higher-order SIE and FEM-MoM techniques, as well as the WIPL-D results. Numerical examples have demonstrated that the double-higher-order VIE and VSIE modeling provides a useful alternative to other, more frequently used, types of CEM techniques and either on par or a more efficient solution in many cases, even when compared to techniques implementing similar types of higher order numerical discretization. It has also been demonstrated that both components of the double-higher-order VIE/SIE modeling, i.e., higher order geometrical modeling and higher order current modeling, are essential for accurate and efficient MoM-VSIE computations.

References

[1] R. F. Harrington, *Field Computation by Moment Methods*. Piscataway: IEEE Press, 1993.

[2] B. M. Kolundžija and A. R. Djordjević, *Electromagnetic Modeling of Composite Metallic and Dielectric Structures*. Norwood, MA: Artech House, 2002.

[3] A. F. Peterson, *Mapped Vector Basis Functions for Electromagnetic Integral Equations*. New York, NY, USA: Morgan & Claypool Publishers, 2006.

[4] *Fast and Efficient Algorithms in Computational Electromagnetics*, W. C. Chew, J. M. Jin, E. Michielssen, and J. M. Song, Eds. Norwood, MA, USA: Artech House, 2001.

[5] J. L. Volakis and K. Sertel, *Integral Equation Methods for Electromagnetics*. Raleigh, NC, USA: SciTech Publishing, 2011.

[6] S. M. Rao, T. K. Sarkar, P. Midya, and A. R. Djordjević, "Electromagnetic radiation and scattering from finite conducting and dielectric structures: Surface/surface formulation," *IEEE Trans. Antennas Propag.*, vol. 39, no. 7, pp. 1034–1037, Jul. 1991.

[7] A. I. Mackenzie, S. M. Rao, and M. E. Baginski, "Method of moments solution of electromagnetic scattering problems involving arbitrarily-shaped conducting/dielectric bodies using triangular patches and pulse basis functions," *IEEE Trans. Antennas Propag.*, vol. 58, pp. 488–493, Dec. 2009.

[8] D. H. Schaubert, D. R. Wilton, and A. W. Glisson, "A tetrahedral modeling method for electromagnetic scattering by arbitrarily shaped inhomogeneous dielectric bodies," *IEEE Trans. Antennas Propag.*, vol. AP-32, pp. 77–85, Jan. 1984.

[9] T. K. Sarkar, E. Arvas, and S. Ponnapalli, "Electromagnetic scattering from dielectric bodies," *IEEE Trans. Antennas Propag.*, vol. 37, pp. 673–676, May 1989.

[10] B. J. Rubin and S. Daijavad, "Radiation and scattering from structures involving finite-size dielectric regions," *IEEE Trans. Antennas Propag.*, vol. 38, pp. 1863–1873, Nov. 1990.

[11] P. Zwamborn and P. M. van den Berg, "The three-dimensional weak form of the conjugate gradient FFT method for solving scattering problems," *IEEE Trans. Microw. Theory Techn.*, vol. 40, pp. 1757–1766, Sep. 1992.

[12] T. K. Sarkar and E. Arvas, "An integral equation approach to the analysis of finite microstrip antennas: Volume/surface formulation," *IEEE Trans. Antennas Propag.*, vol. 38, pp. 305–312, Mar. 1990.
[13] A. J. Parfitt, D. W. Griffin, and P. H. Cole, "On the modeling of metal strip antennas contiguous with the edge of electrically thick finite size dielectric substrates," *IEEE Trans. Antennas Propag.*, vol. 40, pp. 134–140, Feb. 1992.
[14] S. N. Makarov, S. D. Kulkarni, A. G. Marut, and L. C. Kempel, "Method of moments solution for a printed patch/slot antenna on a thin finite dielectric substrate using the volume integral equation," *IEEE Trans. Antennas Propag.*, vol. 54, pp. 1174–1184, Apr. 2006.
[15] B. M. Notaroš, "Higher order frequency-domain computational electromagnetics," *IEEE Trans. Antennas Propag.*, vol. 56, pp. 2251–2276, Aug. 2008.
[16] G. Kang, J. Song, W. C. Chew, K. C. Donepudi, and J. M. Jin, "A novel grid-robust higher order vector basis function for the method of moments," *IEEE Trans. Antennas Propag.*, vol. 49, pp. 908–915, June 2001.
[17] M. Djordjević and B. M. Notaroš, "Double higher order method of moments for surface integral equation modeling of metallic and dielectric antennas and scatterers," *IEEE Trans. Antennas Propag.*, vol. 52, pp. 2118–2129, Aug. 2004.
[18] W. Cai, T. Yu, H. Wang, and Y. Yu, "High-order mixed RWG basis functions for electromagnetic applications," *IEEE Trans. Microw. Theory Tech.*, vol. 49, no. 7, pp. 1295–1303, July 2001.
[19] S. Wandzura, "Electric-current basis functions for curved surfaces," *Electromagn.*, vol. 12, no. 1, pp. 77–91, 1992.
[20] B. D. Popović and B. M. Notaroš, "Entire-domain polynomial approximation of volume currents in the analysis of dielectric scatterers," *IEE Proc.—Microw., Antennas Propag.*, vol. 142, no. 3, pp. 207–212, June 1995.
[21] B. M. Notaroš and B. D. Popović, "General entire-domain method for analysis of dielectric scatterers," *IEE Proc.—Microw., Antennas Propag.*, vol. 143, no. 6, pp. 498–504, Dec. 1996.
[22] B. M. Notaros and B. D. Popovic, "Optimized entire-domain moment-method analysis of 3D dielectric scatterers," *Int. J. Numer. Modelling: Electronic Networks, Devices Fields*, vol. 10, pp. 177–192, 1997.
[23] B. M. Notaros and B. D. Popovic, "General entire-domain Galerkin method for analysis of wire antennas in the presence of dielectric bodies," *IEE Proc.—Microw., Antennas Propag.*, vol. 145, no. 1, pp. 13–18, Feb. 1998.
[24] P. De Doncker, "A potential integral equations method for electromagnetic scattering by penetrable bodies," *IEEE Trans. Antennas Propag.*, vol. 49, pp. 1037–1042, Jul. 2001.
[25] K. Sertel and J. L. Volakis, "Method of moments solution of volume integral equations using parametric geometry modeling," *Radio Sci.*, vol. 37, pp. 10-1–10-7, Jan.–Feb. 2002.
[26] O. S. Kim, P. Meincke, O. Breinbjerg, and E. Jørgensen, "Method of moments solution of volume integral equations using higher-order hierarchical Legendre basis functions," *Radio Sci.*, vol. 39, pp. 1–7, Sept. 2004, RS5003.
[27] M. M. Botha, "Solving the volume integral equations of electromagnetic scattering," *J. Computat. Phys.*, vol. 218, pp. 141–158, 2006.
[28] M. M. Botha, "Fully hierarchical divergence-conforming basis functions on tetrahedral cells, with applications," *Int. J. Numer. Meth. Eng.*, vol. 71, pp. 127–148, 2007.
[29] R. D. Graglia and A. F. Peterson, "Hierarchical divergence-conforming Nédélec elements for volumetric cells," *IEEE Trans. Antennas Propag.*, vol. 60, no. 11, pp. 5215–5227, Nov. 2012.
[30] B. M. Notaroš and B. D. Popović, "Large-domain integral-equation method for analysis of general 3-D electromagnetic structures," *IEE Proc.—Microw., Antennas Propag.*, vol. 145, no. 6, pp. 491–495, Dec. 1998.
[31] B. M. Notaroš, B. D. Popović, J. P. Weem, R. A. Brown, and Z. Popović, "Efficient large-domain MoM solutions to electrically large practical EM problems," *IEEE Trans. Microw. Theory Tech.*, vol. 49, pp. 151–159, Jan. 2001.
[32] B. M. Notaroš and B. D. Popović, "Generalized excitations and loads for 3D electromagnetic analysis with boundary elements (Invited Paper)," *Int. J. Eng. Analysis With Boundary Elements, ELSEVIER*, vol. 27, pp. 333–343, Apr. 2003.
[33] S. D. Gedney and C. C. Lu, "High-order integral equation solution for scattering by composite materials," in *Proc. 2003 IEEE Antennas Propag. Soc. Int. Symp. Dig.*, Columbus, OH, USA, Jun. 22–27, 2003, vol. 2, pp. 1055–1058.
[34] O. S. Kim, P. Meincke, O. Breinbjerg, and E. Jørgensen, "Solution of volume-surface integral equations using higher-order hierarchical Legendre basis functions," *Radio Sci.*, vol. 42, pp. 1–8, Aug. 2007, RS4023.
[35] J. L. Volakis, K. Sertel, and B. C. Usner, *Frequency Domain Hybrid Finite Element Methods in Electromagnetics*. New York, NY, USA: Morgan & Claypool Publishers, 2006.
[36] J. Liu and J. M. Jin, "A novel hybridization of higher order finite element and boundary integral methods for electromagnetic scattering and radiation problems," *IEEE Trans. Antennas Propag.*, vol. 49, pp. 1794–1806, Dec. 2001.
[37] M. M. Ilić and B. M. Notaroš, "Higher order hierarchical curved hexahedral vector finite elements for electromagnetic modeling," *IEEE Trans. Microw. Theory Tech.*, vol. 51, pp. 1026–1033, Mar. 2003.
[38] R. D. Graglia and A. F. Peterson, "Hierarchical curl-conforming Nédélec elements for quadrilateral and brick cells," *IEEE Trans. Antennas Propag.*, vol. 59, no. 8, pp. 2766–2773, Aug. 2011.
[39] E. M. Klopf, N. J. Sekeljic, M. M. Ilic, and B. M. Notaros, "Optimal modeling parameters for higher order MoM-SIE and FEM-MoM electromagnetic simulations," *IEEE Trans. Antennas Propag.*, vol. 60, no. 6, pp. 2790–2801, 2012.
[40] M. Djordjević and B. Notaroš, "Higher-order hierarchical basis functions with improved orthogonality properties for moment-method modeling of metallic and dielectric microwave structures," *Microw. Opt. Technol. Lett.*, vol. 37, no. 2, pp. 83–88, Apr. 2003.
[41] M. M. Kostić and B. M. Kolundžija, "Maximally-orthogonalized higher order bases over generalized wires, quadrilaterals, and hexahedra," *IEEE Trans. Antennas Propag.*, vol. 61, no. 6, pp. 3135–3148, Jun. 2013.
[42] M. M. Ilić, M. Djordjević, A. Ž. Ilić, and B. M. Notaroš, "Higher order hybrid FEM-MoM technique for analysis of antennas and scatterers," *IEEE Trans. Antennas Propag.*, vol. 57, pp. 1452–1460, May 2009.
[43] R. W. Ziolkowski and M. Tanaka, "FDTD analysis of PBG waveguides, power splitters and switches," *Opt. Quantum Electron.*, vol. 31, pp. 843–855, 1999.
[44] A. Bingham, Y. Zhao, and D. Grischkowskya, "THz parallel plate photonic waveguides," *Appl. Phys. Lett.*, vol. 87, pp. 1–3, 2005, 051101.
[45] X. Xiaoli and X. Jiaotong, "FDTD simulation of interstitial antenna for bone cancer microwave hyperthermic therapy," in *Proc. 2004 IEEE Antennas Propag. Soc. Int. Symp.*, Monterey, CA, USA, Jun. 20–25, 2004.

Elene Chobanyan (S'12) was born in Tbilisi, Georgia, in 1986. She received the B.S. degree in physics and the M.S. degree in electrical and electronics engineering from Tbilisi State University, Tbilisi, Georgia, in 2007 and 2009, respectively. Since 2010, she has been a Research Assistant in Electromagnetics Laboratory in the Department of Electrical and Computer Engineering, at Colorado State University, Fort Collins, CO, USA, where she is currently working towards her Ph.D. degree.

From 2006 to 2010, she worked in the R&D department at EMCoS in Tbilisi, Georgia. As a member of EM Methods Development Department, she was primarily dealing with computational techniques such as Method of Moments (MoM), Method of Auxiliary Sources (MAS), Transmission Line Methods and Network Analysis. In 2008 she was an EMCoS representative at "JSOL Corporation" (former JRI Solutions, Ltd.) in Tokyo, Japan. In summer 2013 she was an intern in engineering simulation software developer ANSYS Inc. in Boulder, Colorado. Her research interests include computational electromagnetics, antennas, scattering and circuits.

Milan M. Ilić (S'00–M'04) was born in Belgrade, Serbia, in 1970. He received the Dipl. Ing. and M.S. degrees in electrical engineering from the University of Belgrade, Serbia, in 1995 and 2000, respectively, and the Ph.D. degree from the University of Massachusetts Dartmouth, MA, USA, in 2003.

He is currently an Associate Professor in the School of Electrical Engineering at the University of Belgrade and a postdoctoral Research Associate and Affiliated Faculty with the ECE department of the Colorado State University, USA. His research

interests include computational electromagnetics, antennas, and microwave components and circuits.

Dr. Ilić served as Technical Program Committee Chair for the 11th International Workshop on Finite Elements for Microwave Engineering—FEM2012, June 4–6, 2012, Estes Park, Colorado, USA. He was the recipient of the 2005 IEEE MTT-S Microwave Prize.

Branislav M. Notaroš (M'00–SM'03) was born in Zrenjanin, Yugoslavia, in 1965. He received the Dipl. Ing. (B.S.), M.S., and Ph.D. degrees in electrical engineering from the University of Belgrade, Belgrade, Yugoslavia, in 1988, 1992, and 1995, respectively.

From 1996 to 1999, he was an Assistant Professor in the School of Electrical Engineering at the University of Belgrade. He spent the 1998–1999 academic year as a Visiting Scholar at the University of Colorado at Boulder. He was an Assistant Professor, from 1999 to 2004, and Associate Professor, from 2004 to 2006, in the Department of Electrical and Computer Engineering at the University of Massachusetts Dartmouth. From 2006 to 2012, he was an Associate Professor in the Department of Electrical and Computer Engineering at Colorado State University, where he is currently a Professor and Director of Electromagnetics Laboratory. His research interests and activities are in computational electromagnetics, antennas, scattering, microwaves, and metamaterials, and in particular in higher order computational electromagnetic techniques based on the method of moments, finite element method, physical optics, domain decomposition method, diakoptics, and hybrid methods as applied to modeling and design of antennas, scatterers, and microwave and optical devices. His publications include more than 100 journal and conference papers, and three workbooks in electromagnetics and in fundamentals of electrical engineering (basic circuits and fields). He is the author of textbooks *Electromagnetics* (Prentice Hall, 2010) and *MATLAB-Based Electromagnetics* (Prentice Hall, 2013), as well as the Electromagnetics Concept Inventory (EMCI).

Dr. Notaroš served as General Chair for the 11th International Workshop on Finite Elements for Microwave Engineering—FEM2012, June 4–6, 2012, Estes Park, CO, USA. He was the recipient of the 2005 IEEE MTT-S Microwave Prize (best-paper award for IEEE Transactions on MTT), 1999 IEE Marconi Premium (best-paper award for IEE Proceedings on Microwaves, Antennas and Propagation), 1999 URSI Young Scientist Award, 2005 UMass Dartmouth Scholar of the Year Award, 2004 UMass Dartmouth College of Engineering Dean's Recognition Award, 1992 Belgrade Chamber of Industry and Commerce Best M.S. Thesis Award, 2009, 2010, and 2011 Colorado State University Electrical and Computer Engineering Excellence in Teaching Awards, 2010 Colorado State University College of Engineering George T. Abell Outstanding Teaching and Service Faculty Award, 2012 Colorado State University System Board of Governors Excellence in Undergraduate Teaching Award, and 2013 IEEE Region 5 Outstanding Engineering Educator Award.